JOURNAL OF THERMOPHYSICS AND HEAT TRANSFER
Vol. 13, No. 4, October-December 1999

Effective Thermal Conductivity of Graphite–Metallic Salt Complex for Chemical Heat Pumps

Jong Hun Han* and Kun-Hong Lee†
Pohang University of Science and Technology, Kyung Buk 790-784, Republic of Korea
and
Hwayong Kim‡
Seoul National University, Seoul 151-742, Republic of Korea

An experimental procedure was developed for measuring the effective thermal conductivities of graphite-$CaCl_2 \cdot n NH_3$ ($n = 8, 4, 2$), graphite-$MnCl_2 \cdot n NH_3$ ($n = 6, 2$), and graphite-$BaCl_2 \cdot 8NH_3$ complex for chemical heat pumps. Graphite-metallic salt complex was manufactured through the impregnation of metallic salt into a porous graphite matrix. Experimental conditions of pressure and temperature were directly established by the thermodynamic equilibrium lines of salt–ammonia systems obtained by the calorimetric method. Afterward, effective thermal conductivities were measured using a transient one-dimensional heat flow technique at a fixed pressure and temperature under an ammonia atmosphere. Effective thermal conductivities of the graphite-metallic salt complex were in the range of 10–49 W/mK, which are significant higher values than powder beds of 0.1–0.5 W/mK. Results showed that the effective thermal conductivity of a graphite-metallic salt complex has a strong dependency on the bulk density, the weight fraction of graphite, and the ammoniated state of salt.

Nomenclature

C = width of specimen, m
C_p = heat capacity, J/kg-K
D = thickness of specimen, m
e_b = thickness of complex, m
e_w = thickness of wall, m
f_g = weight fraction of graphite, %
G = working fluid
h_f = heat transfer coefficient of thermal fluid, W/m^2-K
h_L = heat transfer coefficient at specimen surface, W/m^2-K
I_0 = initial current, A
k_e = effective thermal conductivity, W/m-K
k_f = thermal conductivity of ammonia, W/m-K
L = length of specimen, m
MW_s = molecular weight of anhydrous salt, kg/mol
m_g = mass of graphite, kg
P_c = constraint pressure, bar
Q_0 = heat production by thermistor, W
q_s = heat flux by thermistor, W/m^2
R = resistance of thermistor, Ω
R_c = residual resistance by external circuit, Ω
R_v = resistance of varistor, Ω
R_0 = initial resistance of thermistor, Ω
S = external surface area of specimen, m^2
T = temperature, K
T_a = ambient temperature, K
T_c = constraint temperature, K
T_s = surface temperature of specimen, K
T_0 = initial temperature, K
t = time, s
U = applied voltage, V
U_p = overall heat transfer coefficient, W/m^2-K
V_b = volume of graphite-metallic salt complex, m^3
V_s = volume occupied by salt in complex, m^3
v_s = molar volume of salt, m^3/mol
w = dimensionless number
α_e = thermal diffusivity, m^2/s
β = volumetric coefficient of expansion, K^{-1}
γ = temperature coefficient of thermistor, K^{-1}
ΔT_c = temperature drop at boundary, K
ΔT_p = degree of pseudo-equilibrium domain, K
Θ = characteristic time, s
ν = kinematic viscosity of ammonia, m^2/s
ρ = density, kg/m^3
σ = Stefan–Boltzmann constant, W/m^2-K^4
ϕ = porosity
φ = Prandtl number function

Introduction

SOLID–GAS reversible reactions have been widely applied in energy processes such as chemical heat pump (CHP), thermal storage, cooler-heater, etc.[1–5] Metallic salts–ammonia can be utilized as a solid-gas reaction pair for the heat and cold production over wide range of −30–350°C (Ref. 1). The performance of CHPs based on a number of metallic salt–ammonia reactions is greatly influenced by the efficiency of heat and mass transfer in a fixed bed reactor. However, reaction beds made of these metallic salts have very low effective thermal conductivity of 0.1–0.5 W/mK due to the low intrinsic thermal conductivity of inorganic salts and poor contacts between particles. Furthermore, diffusion of ammonia within the reaction bed is impeded by pore clogging due to the volume expansion or swelling of the salt during the synthesis reaction of ammonia and metallic salt. Accordingly, low thermal power density and low coefficient of performance of CHPs are obtained.

Use of a heat conductive medium can improve heat transfer and, consequently, the dynamics of reactor transformation. A porous graphite matrix that is consolidated from expanded graphite powders can be used as a heat conductive medium and is known to be superior to porous metallic foams made of aluminum, copper, or nickel.[6,7] In particular, the graphite-metallic salt complex invented by Mauran et al.[8] has been known to be a very effective reaction bed with effective thermal conductivity of 5–40 W/mK and gas permeability of 10^{-13}–10^{-15} m^2. Knowledge of the effective thermal

Received 12 March 1999; revision received 21 June 1999; accepted for publication 23 June 1999.

*Research Associate, Department of Chemical Engineering, San 31, Hyoja-Dong, Nam-Gu, Pohang.
†Associate Professor, Department of Chemical Engineering, San 31, Hyoja-Dong, Nam-Ku, Pohang.
‡Associate Professor, Department of Chemical Engineering, San 56-1, Sinlim-Dong, Kwanak-Ku.

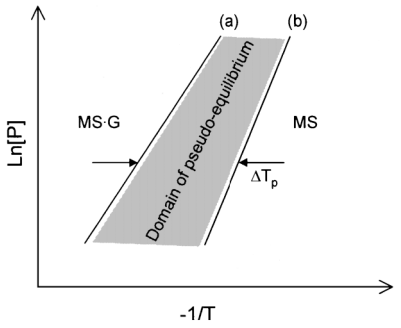

Fig. 1 Thermodynamic equilibrium lines of the solid–gas couple in Clapeyron's diagram, where a indicates pseudo-equilibrium line of synthesis and b indicates pseudo-equilibrium line of decomposition.

conductivity is necessary for accurate heat transfer analysis and dynamic simulation of a reactor, though such data are available for a few salts in the relevant literature. Mauran et al. reported the effective thermal conductivity of graphite–$MnCl_2 \cdot n NH_3$ ($n = 6, 2$) as a function of the bulk density using the transient hot wire method. However, they did not reveal the influence of the relative proportion of graphite powder in the complex on the effective thermal conductivity despite its importance. Therefore, the effective thermal conductivity of graphite–metallic salt complex as a function of the bulk density, the weight fraction of graphite, and the ammoniated state of metallic salt (MS) is not fully understood because the measurements are very difficult in the presence of chemical reactions.

The effective thermal conductivity should be measured under a constraint condition of pressure P and temperature T outside of the pseudo-equilibrium domain. Synthesis and decomposition reactions used in CHPs can be typically represented by a chemical reaction of the following type:

$$\mathrm{MS} + G \Leftrightarrow \mathrm{MS} \cdot G + \Delta H_r \tag{1}$$

For many other MS–ammonia couples, a domain of pseudo equilibrium commonly exists due to weak reactive phases within the MS,[1] and the domain is characterized by the zone between the synthesis line and the decomposition line, as shown in Fig. 1. In this domain, the reaction rate is almost zero.[9] Thus, synthesis or decomposition of the ammoniated salts practically occurs outside of the pseudo-equilibrium domain, though the exact position of the true equilibrium line lies within this domain. For these reasons, the correct characterization of pseudo-equilibrium domain is very important in case we know the ammoniated state of MSs, from P and T conditions. In this paper, thermodynamic equilibrium lines for the systems of NH_3–$CaCl_2$, $MnCl_2$, and $BaCl_2$ were obtained using a calorimetric method to establish experimental conditions of P and T for the measurements. The effective thermal conductivity of graphite–$CaCl_2 \cdot n NH_3$ ($n = 8$, 4, and 2), $MnCl_2 \cdot n NH_3$ ($n = 6$ and 2) and $BaCl_2 \cdot 8NH_3$ complex were measured using the transient one-dimensional heat flow technique.

Theoretical Background of Thermal Conductivity Measurement

Because the MS is hygroscopic and incoherent contacts between the heat source and the graphite–MS complex may occur due to the volume expansion of the complex under an ammonia atmosphere, the measurement of thermal conductivity should only be done using a purpose-built apparatus. In particular, ammonia gas causes serious corrosion on metal surfaces such as copper, which makes it impossible to use ordinary apparatus for the thermal conductivity measurement. The transient one-dimensional heat flow technique was proposed as a simple and reasonably accurate method to measure effective thermal conductivity under various operating conditions.[10] Measurement was done by heating the specimen surface continuously and simultaneously recording the temperature at the same surface as a function of time. In this method, temperature variation of the heat source can be within 5°C, and the measurement time is

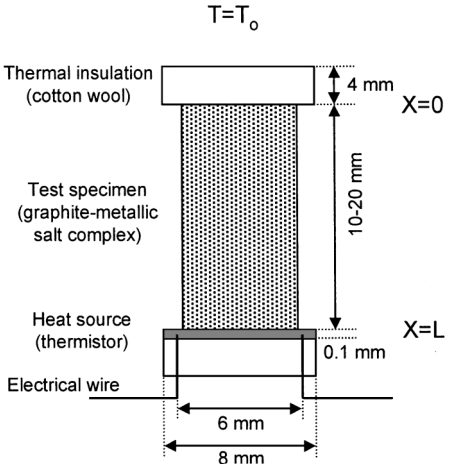

Fig. 2 Experimental setup for the thermal conductivity measurements.

5–10 s. These conditions are very important to completely remove the enthalpy effect of chemical reactions that may be introduced due to the long duration of heat applied to the graphite–MS complex. Therefore, this method can even be applied to porous reactive media with the narrow P–T equilibrium domain between consecutive solid–gas reactions.

The technique presented in this work makes use of a thermistor of extremely small thickness compared to the length of the test specimen. Figure 2 shows the experimental setup for the thermal conductivity measurement. A direct voltage is applied to the thermistor for about 5–10 s, to raise the temperature of the thermistor by 2–3°C. The resistance of the thermistor varies due to temperature increase, and there occurs a corresponding change of voltage drop. By recording the voltage variation over a certain time period from the onset of the heating current, it is possible to obtain precise information on the heat flow between the thermistor and the test specimen. It is assumed that the heat capacity of the thermistor can be negligible compared to the heat capacity of the test specimen and that there is no loss of heat at the surface of the specimen.

Consider the specimen as a slab of thickness L initially at a uniform temperature T_0. The face at $x = 0$ is perfectly insulated, as shown in Fig. 2. At time $t = 0$, a constant heat flux q_s is imposed on the face at $x = L$. The governing differential equation to be solved is then expressed as

$$\frac{\partial T}{\partial t} = \alpha_e \frac{\partial^2 T}{\partial^2 x}, \qquad 0 < x < L \tag{2}$$

The initial and boundary conditions can be also expressed as

$$t = 0, \qquad T = T_0 \tag{3}$$

$$x = L, \qquad -k_e \frac{\partial T}{\partial x} = q_s \tag{4}$$

$$x = 0, \qquad \frac{\partial T}{\partial x} = 0 \tag{5}$$

The temperature response at time t as the solution of Eqs. (2–5) can be given as[11]

$$T(t) - T_0 = \frac{q_s t}{\rho c_p L} + \frac{q_s L}{k_e}\left[\frac{3x^2 - L^2}{6L^2} - \frac{2}{\pi^2}\sum_{n=1}^{\infty}\frac{(-1)^n}{n^2}\exp\left(\frac{-n^2\pi^2\alpha_e t}{L^2}\right)\cos\left(\frac{n\pi x}{L}\right)\right] \tag{6}$$

By the setting of $\rho C_p = k_e/\alpha_e$, the temperature distribution at the boundary of the heat source and the specimen, $x = L$, can be given as

$$T(t) - T_0 = (q_s L/k_e) f(w) \tag{7a}$$

where

$$f(w) = w + \frac{1}{3} - \frac{2}{\pi^2}\sum_{n=1}^{\infty} n^{-2}\exp(-n^{-2}\pi^2 w) \tag{7b}$$

$$w = \frac{\alpha t}{L^2} = \frac{t}{\Theta} \tag{7c}$$

There is a finite temperature drop ΔT_c due to incomplete thermal contact between the thermistor and the surface of the specimen. Because the heat liberation of the thermistor is almost constant during measurement, ΔT_c rapidly approaches a constant value. In fact, the time period needed to establish ΔT_c is less than the gap thickness squared divided by the thermal diffusivity of the gap material, that is, a few micrometer of ammonia or an electrically insulating layer of known thickness. Thus, the temperature response of the thermistor is then expressed as

$$T(t) - T_0 = \Delta T_c + (q_s L/k_e) f(w) \tag{8}$$

and, from the temperature-resistivity relationship of the thermistor, the resistivity variation of the themistor can be given as

$$R(t) = A + B \cdot f(w) \tag{9a}$$

where

$$A = R_0(1 + \gamma \Delta T_c) \tag{9b}$$

$$B = R_0 \gamma (Q_0 L / C D k_e) \tag{9c}$$

The effective thermal conductivity can be derived from slope B through the linear regression of $R(t)$ vs $f(w)$ curve through the iteration process by varying Θ.

Thermodynamic Equilibrium of MS–Ammonia Couples

Thermodynamic equilibrium lines on the relationship of P–T were obtained using a pressure differential scanning calorimeter from TA Instruments with temperature repeatability of ± 0.1°C and calorimetric sensitivity of 1 μW. About 3 mg of pure metallic salt was loaded on the measuring cell and was dehydrated at 160–200°C under a vacuum to remove the water and the air within the salt and the cell. The pressure of the measuring cell that was connected to an ammonia gas (Solkatronic, 99.995%) supply was kept constant during each measurement by the back pressure regulator (TESCOM, 100 psig). The pressure in the cell was set in the range of 1.0–5.0 bar. The synthesis reaction between the MS and the ammonia was induced by introducing ammonia gas into the measuring cell at a fixed P_c and T_c. The flow of ammonia gas was continuous up to the completion of an experiment. The temperature of the salt in the measuring cell increased due to the heat of reaction by exothermic reaction. Afterward, it was maintained until the temperature of salt fell to T_c. Under a constant P_c, the temperature was programmed to increase at a rate of 0.5°C/min from T_c. Simultaneously, by recording the thermal flux delivered over the cell, it was possible to obtain the temperature corresponding to the decomposition reaction. After the completion of the decomposition reaction, the temperature of the cell was gradually decreased again to T_c, recording the thermal flux with the cell temperature together. This also allowed the temperature corresponding to the synthesis reaction to be obtained. The reaction pairs investigated were $CaCl_2$, $MnCl_2$, and $BaCl_2$–NH_3.

Preparation of Graphite–MS Complex

Expandable graphite powders (imported from the People's Republic of China) with particle size of 420–500 μm were selected using sieve analysis. They were dried in a circulation oven at 60°C for 10 h to remove moisture before heat treatment. Heat treatment was performed by inserting the steel crucible containing about 3 g of expandable graphite powders into the furnace (from Fisher, coal analyzer 490) and maintaining a constant temperature of 700°C for 2 min in air atmosphere. Expansion and exfoliation of graphite powders occurs during the heat treatment. The expanded graphite powders were poured into a cylindrical mold of hardened steel, then pressed by a single acting platen to obtain the porous graphite matrix with preferred bulk density. Graphite–MS complexes were prepared using an impregnation method. Aqueous solutions of $CaCl_2$ (Aldrich, 22,231-1), $MnCl_2$ (Shinyo, 98.5%), and $BaCl_2$ (Samchun, 98%) of 20–30 wt % concentrations were prepared with H_2O as a solvent. A porous graphite matrix was placed in a container filled with one of the three salt solutions. A vacuum of about 0.018 bar was applied into the container for several minutes to soak the porous graphite matrix in the salt solution. The soaked graphite complex was dried in a circulation oven at 60–80°C, followed by vacuum drying (Precision Scientific, Inc., Model 5831) at >200°C for 3 h.

Two parameters used to identify the graphite–salt complex are

$$\rho_b = m_g / V_b \tag{10a}$$

$$f_g = m_g / (m_{\text{salt}} + m_g) \tag{10b}$$

Measurement of Effective Thermal Conductivity

Figure 3 shows a schematic diagram of the apparatus for the thermal conductivity measurements. The graphite–salt metallic complex was used as a specimen. The specimen was placed on top of the thermistor (Measurement Group, Model ET-TG-AAU-00500), which functioned as a temperature sensor and a heat source. The specimen was fixed by a steel clamp to keep secure contact between the thermistor and the specimen. Resistance of the thermistor was 50 Ω ±0.3% at 24°C, and the temperature change was sensed by the resistance change of the thermistor. A vacuum of about 10^{-4} torr was applied to remove the air and the moisture in the cell. Initially, the temperature of the specimen was stabilized at a fixed temperature for about 30 min. Temperature of the cell was controlled by the precision thermostatic bath (Fisher Scientific, Model 9010) with stability of ±0.1°C. Resistance of the varistor (maximum 100 Ω) was set to equate with the resistance of the thermistor corresponding to the fixed temperature. This enables heat flux Q_0 to be constant during heating. The pressure of the ammonia

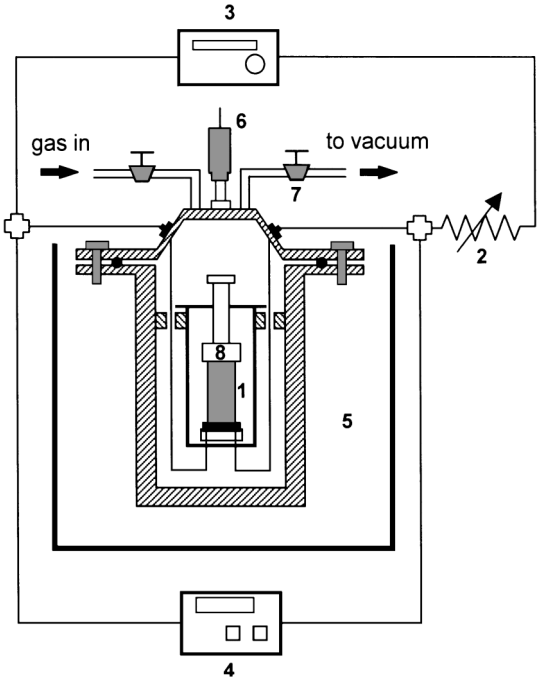

Fig. 3 Schematic diagram of the apparatus for thermal conductivity measurements: 1, graphite–metallic salt complex; 2, variable resistor; 3, power supply; 4, digital multimeter; 5, thermostatic bath; 6, pressure transducer; 7, metering valve; and 8, thermal insulating material.

Table 1 Experimental conditions for thermal conductivity measurements

Ammoniated state	Pressure, bar	Temperature, °C
$CaCl_2 \cdot 8NH_3$	1.7–2.5	30
$CaCl_2 \cdot 4NH_3$	1.7–2.8	60
$CaCl_2 \cdot 2NH_3$	1.7–2.3	85
$MnCl_2 \cdot 6NH_3$	1.2–2.2	50
$MnCl_2 \cdot 2NH_3$	1.2–3.0	120
$BaCl_2 \cdot 8NH_3$	3.4–5.0	20

gas in the cell was measured by a pressure transducer (Valcom, Model VPRN-5K). Table 1 shows the experimental conditions for the thermal conductivity measurements of the graphite-ammoniated salt complex. Direct voltage of 7.00 V generated by the power supply (Hewlett Packard, Model HP6033A) was applied to the thermistor for 5–10 s to raise the temperature about 2–3°C. The voltage change between two ends of the thermistor was read by the precision digital multimeter (Hewlett Packard, Model HP34401A) and transferred via an HPIB interface board to the personal computer, which converted measured voltage into the resistance changes by

$$R(t) = \frac{R_s U(t)}{U_{\text{tot}} - U(t)} \tag{11}$$

The initial current and Q_0 were calculated by

$$I_0 = \frac{U_{\text{tot}}}{(R_0 + R_v + R_c)} \tag{12a}$$

$$Q_0 = I_0^2 \cdot R_0 \tag{12b}$$

Reliability of our equipment was confirmed by checking with the thermal conductivity of the stainless steel (Standard Reference Materials NIST 1462, 14.2 ± 0.4 W/mK). A series of five measurements using our equipment was carried out with the standard reference material. Average value of our measurements was 13.9 ± 0.2 W/mK, which was in good agreement with the value given from NIST.

The temperature coefficient of the thermistor was determined by measuring its resistance as a function of temperature in the range of −15–150°C. A second-order equation was fitted to the measured resistance with temperature, then the temperature (Kelvin) coefficient was calculated by

$$R(T) = -0.692 + 0.0797 \cdot T + 3.059 \cdot 10^{-4} \cdot T^2 \tag{13a}$$

$$\gamma = \frac{1}{R}\frac{\partial R}{\partial T} \tag{13b}$$

It is important to keep $w_{\max}$ in Eq. (7c) (for the last measurement time) in the range of 0.5–1.0 for reliable results within the measurement time of 5–10 s (Ref. 10). Slope B in Eq. (9c) is dependent on the finite specimen size of L. Thus, the approximate thermal diffusivity should be known a priori to determine the length of the specimen, which is satisfactory to $0.5 < w_{\max} < 1.0$. Thermal diffusivity of graphite–MS complex was measured to determine the appropriate specimen length using the laser flash method (THETA, Inc.). The appropriate length of graphite–MS complex was in the range of 10–20 mm.

Results and Discussion

To investigate the effect of the ammoniated states of the salts on the thermal conductivity, measurement must be carried out under conditions where the composition or the state of the salt particles does not vary during the experiment by taking into account the two thermodynamic constraints of P_c and T_c. Different equilibrium lines in several degrees Celsius have been reported, depending on different authors using various methods. Therefore, accurate data of the equilibrium lines are necessary in advance of measurements.

A calcium chloride–ammonia system is selected because it has been used in commercial sorption refrigeration units with some excellent results. It is also considered for solar cooling, cooling on trains, refrigeration in tropical climates, and in a system for high-temperature heat storage for power generation.[12] Figure 4 shows the thermodynamic equilibrium lines for $CaCl_2$–NH_3 system on Clapeyron's diagram. Lines a, b, and c in Fig. 4 are related to the following chemical reactions: Line a is

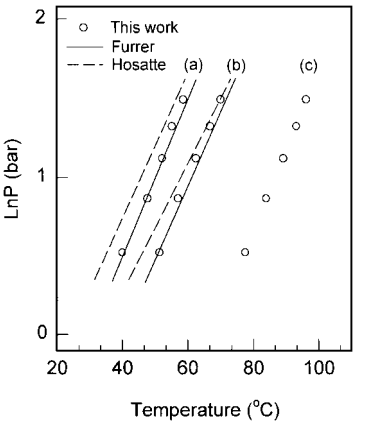

Fig. 4 Thermodynamic equilibrium curves of pressure–temperature for $CaCl_2$–NH_3 system.

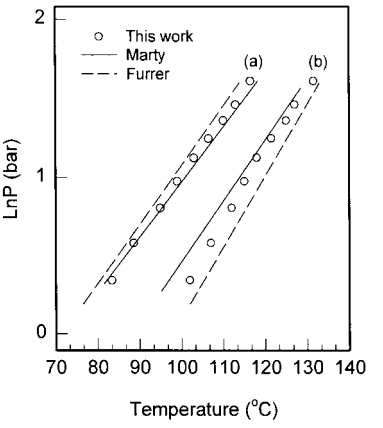

Fig. 5 Thermodynamic equilibrium curves of pressure–temperature for $MnCl_2$–NH_3 system.

$$CaCl_2 + 8NH_3 \Leftrightarrow CaCl_2 \cdot 8NH_3 \tag{14a}$$

Line b is

$$CaCl_2 + 8NH_3 \Leftrightarrow CaCl_2 \cdot 4NH_3 + 4NH_3 \tag{14b}$$

Line c is

$$CaCl_2 + 4NH_3 \Leftrightarrow CaCl_2 \cdot 2NH_3 + 2NH_3 \tag{14c}$$

The equilibrium line a is for the synthesis reaction of $CaCl_2$ that is coordinated with eight ammonia molecules. The equilibrium lines b and c are for the decomposition reactions of $CaCl_2 \cdot 8NH_3$ and $CaCl_2 \cdot 4NH_3$, respectively. The equilibrium lines a and b are similar to Furrer's results,[13] whereas Hosatte and Rheault[14] reported slightly higher equilibrium pressure at a given temperature, as shown in Fig. 4.

From a static design procedure, $MnCl_2$ and $BaCl_2$–NH_3 systems are selected as optimum pairs for cold production of 10°C using the industrial waste heat of 150–160°C. Detailed descriptions of this design procedure are beyond the scope of this study. Figure 5 shows the thermodynamic equilibrium lines for the $MnCl_2$–NH_3 system on Clapeyron's diagram. Lines a and b in Fig. 5 are related to the following chemical reaction:

$$MnCl_2 \cdot 6NH_3 \Leftrightarrow MnCl_2 \cdot 2NH_3 + 4NH_3 \tag{15}$$

The equilibrium lines a and b are for the synthesis reaction of $MnCl_2 \cdot 2NH_3$ and for the decomposition reaction of $MnCl_2 \cdot 6NH_3$, respectively. Marty also reported the equilibrium lines for the

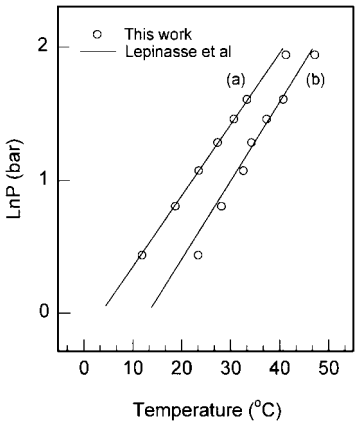

Fig. 6 Thermodynamic equilibrium curves of pressure–temperature for $BaCl_2$–NH_3 system.

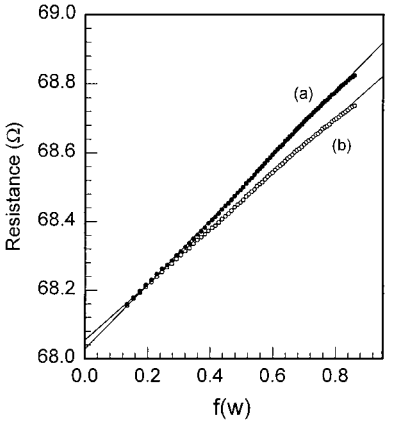

Fig. 7 Plots for obtaining effective thermal conductivity of graphite–$CaCl_2 \cdot 2NH_3$ complex, where line a is ρ_b = 145 kg/m^3 and f_g = 30% and line b is ρ_b = 175 kg/m^3 and f_g = 50%.

$MnCl_2$–NH_3 system obtained by using a differential scanning calorimeter.[15] A difference in the results is observed only at low pressure, less than 2.5 bar, in equilibrium line b. However, Furrer[13] reported somewhat different equilibrium lines in comparison with our results and Marty's results.[15] As for many other solid–gas couples, a domain of pseudo equilibrium is characterized between the synthesis line and the decomposition line. The pseudo-equilibrium domain can be expressed as ΔT_p at a given pressure, as shown in Fig. 1. Usually the value of ΔT_p is more than 5°C for many MS–ammonia pairs. In the case of the $MnCl_2$–NH_3 system, ΔT_p was in the range of 18–22°C at a pressure of 1.0–5.0 bar.

Figure 6 shows the thermodynamic equilibrium lines for the $BaCl_2$–NH_3 system on Clapeyron's diagram. Lines a and b in Fig. 6 are related to the following chemical reaction:

$$BaCl_2 \cdot 8NH_3 \Leftrightarrow BaCl_2 + 8NH_3 \qquad (16)$$

The equilibrium lines a and b are for the synthesis and the decomposition reaction of $BaCl_2 \cdot 8NH_3$ in Eq. (16), respectively. Our results are similar to Lepinasse and Spinner's[16] data, as shown in Fig. 6. In the case of the $BaCl_2$–NH_3 system, ΔT_p is in the range of 7–10°C at a pressure of 1.0–5.0 bar. Therefore, from the pseudo-equilibrium conditions of P–T for the $CaCl_2$, $MnCl_2$, and $BaCl_2$–NH_3 systems in this work, we can safely determine experimental conditions for the measurements shown in Table 1 without inducing the chemical reaction that may be caused by the temperature increment of the thermistor.

Figure 7 shows the linear relationship between $R(t)$ vs $f(w)$ in Eq. (9a). The effective thermal conductivity can be evaluated by Eq. (9c) with the slope of the plot whose correlation coefficients are over 0.9995. Table 2 shows the values of the effective thermal conductivity of the graphite–$CaCl_2 \cdot nNH_3$ complex we obtained. For a powder bed of pure $CaCl_2$, Hosatte and Rheault[14] reported a thermal conductivity of 0.065 W/mK for the $CaCl_2 \cdot 2NH_3$ case, of 0.125 W/mK for the $CaCl_2 \cdot 4NH_3$ case, and 0.145 W/mK for the $CaCl_2 \cdot 8NH_3$ case. For the system of $CaCl_2 \cdot 8NH_3$ powders mixed

Table 2 Effective thermal conductivities of graphite–$CaCl_2 \cdot nNH_3$ complex

ρ_b, kg/m^3	f_g, wt %	States of MS	k_e, W/mK
110	70	$CaCl_2 \cdot 8NH_3$	24.0 ± 0.45
		$CaCl_2 \cdot 4NH_3$	21.2 ± 0.56
		$CaCl_2 \cdot 2NH_3$	18.0 ± 0.21
165	70	$CaCl_2 \cdot 8NH_3$	29.5 ± 0.43
		$CaCl_2 \cdot 4NH_3$	25.6 ± 0.33
		$CaCl_2 \cdot 2NH_3$	23.3 ± 0.31
290	70	$CaCl_2 \cdot 8NH_3$	38.0 ± 0.50
		$CaCl_2 \cdot 4NH_3$	31.9 ± 0.25
		$CaCl_2 \cdot 2NH_3$	29.3 ± 0.10
380	70	$CaCl_2 \cdot 8NH_3$	48.6 ± 0.35
		$CaCl_2 \cdot 4NH_3$	40.2 ± 0.20
		$CaCl_2 \cdot 2NH_3$	35.3 ± 0.22
110	50	$CaCl_2 \cdot 8NH_3$	20.0 ± 0.50
		$CaCl_2 \cdot 4NH_3$	17.1 ± 0.46
		$CaCl_2 \cdot 2NH_3$	15.1 ± 0.30
170	50	$CaCl_2 \cdot 8NH_3$	23.4 ± 0.31
		$CaCl_2 \cdot 4NH_3$	20.1 ± 0.25
		$CaCl_2 \cdot 2NH_3$	17.3 ± 0.15
230	50	$CaCl_2 \cdot 8NH_3$	28.3 ± 0.76
		$CaCl_2 \cdot 4NH_3$	22.6 ± 0.40
		$CaCl_2 \cdot 2NH_3$	21.0 ± 0.21
265	50	$CaCl_2 \cdot 8NH_3$	30.1 ± 0.26
		$CaCl_2 \cdot 4NH_3$	24.7 ± 0.35
		$CaCl_2 \cdot 2NH_3$	22.5 ± 0.21
340	50	$CaCl_2 \cdot 8NH_3$	32.5 ± 0.50
		$CaCl_2 \cdot 4NH_3$	28.2 ± 0.20
		$CaCl_2 \cdot 2NH_3$	25.0 ± 0.15
105	30	$CaCl_2 \cdot 8NH_3$	14.1 ± 0.25
		$CaCl_2 \cdot 4NH_3$	11.3 ± 0.20
		$CaCl_2 \cdot 2NH_3$	10.2 ± 0.21
140	30	$CaCl_2 \cdot 8NH_3$	15.2 ± 0.32
		$CaCl_2 \cdot 4NH_3$	13.0 ± 0.20
		$CaCl_2 \cdot 2NH_3$	11.1 ± 0.15
165	30	$CaCl_2 \cdot 8NH_3$	16.1 ± 0.22
		$CaCl_2 \cdot 4NH_3$	13.8 ± 0.15
		$CaCl_2 \cdot 2NH_3$	12.9 ± 0.15

with expanded graphite powders, Valkov[17] reported thermal conductivity of 0.49–0.50 W/mK when $f_g = 12\%$ and of 0.67–0.74 W/mK when $f_g = 25\%$. For system of the graphite–$CaCl_2 \cdot 4NH_3$ mixture, Valkov also reported thermal conductivity of 0.35–0.43 W/mK when $f_g = 12\%$ and of 0.51–0.55 W/mK when $f_g = 25\%$. The thermal conductivity of MS–expanded graphite mixture is somewhat higher than that of the ammoniated salt alone. However, the increase in the thermal conductivity is not prominent when one simply mixes salts and expanded graphite powders. The graphite–salt complex in this work has distinctively higher thermal conductivity than the simple mixture of graphite and salt. When f_g is 70%, the thermal conductivity of the graphite–$CaCl_2 \cdot 2NH_3$ complex was in the range of 18.0–35.3 W/mK with bulk density of 110–380 kg/m^3. The thermal conductivity of the graphite–$CaCl_2 \cdot 4NH_3$ complex was in the range of 21.2–40.2 W/mK, and that of the graphite–$CaCl_2 \cdot 8NH_3$ complex was in the range of 24.0–48.6 W/mK. The large difference in thermal conductivity comes from the different continuity of the graphite phase inside the specimens. The specimen made by Valkov[17] was prepared by simply mixing expanded graphite powders and $CaCl_2$ powders. However, the specimens made by Mauran et al.[8] and in this work are consolidated graphite powders impregnated with MS. Consolidation can provide a continuous heat-conducting path made of graphite, leading to higher conductivity. Accordingly, compared to the effective thermal conductivity of an unconsolidated bed, a noticeable gain of about 100 times was obtained using the graphite–MS complex.

For the graphite–$CaCl_2 \cdot nNH_3$ complex with a fixed ρ_b and f_g, we can also observe that the thermal conductivity depends on the ammoniated state of the MS, which may change the total porosity and MS phase in the complex. Generally, effective thermal conductivity of a solid bed is primarily dependent on the thermal conductivity of continuous phase, the porosity and the structure of the particles,

etc. The total porosity of the graphite–$CaCl_2 \cdot nNH_3$ complex can be expressed as

$$\phi = 1 - (\rho_b/\rho_{\text{graphite}}) - [(1 - f_g)\rho_b/f_g] \cdot (\bar{v}_s/MW_s) \qquad (17)$$

The second term in Eq. (17) is related to the volume fraction of graphite phase. The last term is related to the change of molar volume for the metallic salt. The molar volumes of $CaCl_2 \cdot 8NH_3$, $CaCl_2 \cdot 4NH_3$, and $CaCl_2 \cdot 2NH_3$ are 211.6×10^{-6}, 131.6×10^{-6}, and 91.6×10^{-6} m^3/mol, respectively. The molar volume of MS rapidly increases as the synthesis reaction of the salt–ammonia proceeds. Thus, the pore volume of the graphite–$CaCl_2 \cdot nNH_3$ complex considerably diminishes as the value of n increases, which inevitably induces the reduction of total porosity. When f_g is 70%, the total porosity of the graphite–$CaCl_2 \cdot 2NH_3$ complex was $0.70 < \phi < 0.91$, depending on the bulk density of complex, whereas the total porosity of the graphite–$CaCl_2 \cdot 8NH_3$ complex was $0.52 < \phi < 0.86$. When f_g is 30%, the total porosity of the graphite–$CaCl_2 \cdot 2NH_3$ and the graphite–$CaCl_2 \cdot 8NH_3$ complexes were $0.61 < \phi < 0.75$ and $0.18 < \phi < 0.48$, respectively. Therefore, the decrease of total porosity and the change of salt phase from $CaCl_2 \cdot 2NH_3$ to $CaCl_2 \cdot 8NH_3$ are responsible for the increase in the effective thermal conductivity as the value of n increases.

When f_g is 50%, the thermal conductivity of the graphite–$CaCl_2 \cdot 2NH_3$ complex is in the range of 15.1–25.0 W/mK with bulk density of 110–340 kg/m^3. The thermal conductivity of the graphite–$CaCl_2 \cdot 4NH_3$ complex and the graphite–$CaCl_2 \cdot 8NH_3$ complex are in the range of 17.1–28.2 and of 20.0–32.5 W/mK, respectively. From these results, we know that the effective thermal conductivity decreases as the weight fraction of the salt increases, which comes from the increase of the volume fraction of the MS with the low conducting and discontinuous phase. Because the specific heat of the MS is higher than the graphite, the resulting specific heat of the graphite–salt complex becomes higher as the weight fraction of the salt increases, which induces the decrease of the conductive heat flux by the absorption of heat into the complex. Moreover, there may be a sharper temperature gradient within the complex due to the low thermal diffusivity of the MS. Because the effective thermal conductivity in a specified direction equals the conductive heat flux divided by the negative temperature gradient in that direction, as the weight fraction of salt increases, this leads correspondingly to lower thermal conductivity. Consequently, when f_g is 30%, the thermal conductivity of the graphite–$CaCl_2 \cdot nNH_3$ complex reduces to lower values, as shown in Table 2.

Table 3 shows the effective thermal conductivity of the graphite–$MnCl_2 \cdot nNH_3$ complex. When f_g is 50%, the thermal conductivities of the graphite–$MnCl_2 \cdot 2NH_3$ complex and the graphite–$MnCl_2 \cdot 6NH_3$ complex are in the range of 13.7–21.8 and 14.6–22.9 W/mK, respectively, in the bulk density of 95–235 kg/m^3. The same explanations can be given for the effect of the ammoniated state of salt and the weight fraction of graphite on the thermal conductivity of the graphite–$MnCl_2 \cdot nNH_3$ complex as was given for the graphite–$CaCl_2 \cdot nNH_3$ complex. Mauran et al. have also reported the effective thermal conductivity of the graphite–$MnCl_2 \cdot nNH_3$ complex using the transient hot wire method,[8] which is the only other data known to the authors. Their results are included in Table 3 together with our results. Note that the effective apparent density is defined by Mauran et al. as

$$\rho_x = m_g/[V_b - V_s(x)] \qquad (18a)$$

which is different from our definition [Eq. (9a)]. The volume occupied by the MS, V_s, may strongly vary with the weight fraction of graphite and the ammoniated state of the salt, x. The relationship between ρ_b and ρ_x can be derived from simple arrangements as

$$\rho_x = \{(1/\rho_b) - (v_s/MW_s) \cdot [(1 - f_g)/f_g]\}^{-1} \qquad (18b)$$

The density calculated by Eq. (18b) is also indicated in Table 3 to compare the range of density in this work and the Mauran et al. data. Unfortunately, Mauran et al. did not designate the weight fraction of graphite, which is an important parameter for thermal conductivity. Thus, it is impossible to compare directly the Mauran et al. results with our results. When f_g is 30%, the thermal conductivity of the graphite–$MnCl_2 \cdot 2NH_3$ complex and the graphite–$MnCl_2 \cdot 6NH_3$ complex are in the range of 10.8–12.7 and 11.5–14.1 W/mK, respectively, in bulk density of 90–145 kg/m^3.

Table 3 Effective thermal conductivities of graphite–$MnCl_2 \cdot nNH_3$ complex

ρ_b, kg/m^3	f_g, wt %	MS states	k_e, W/mK	Reference
95(108[a])	50	$MnCl_2 \cdot 6NH_3$	14.6 ± 0.15	This work
(101[a])		$MnCl_2 \cdot 2NH_3$	13.7 ± 0.10	This work
155(193[a])	50	$MnCl_2 \cdot 6NH_3$	16.4 ± 0.40	This work
(172[a])		$MnCl_2 \cdot 2NH_3$	15.7 ± 0.12	This work
180(234[a])	50	$MnCl_2 \cdot 6NH_3$	20.3 ± 0.25	This work
(204[a])		$MnCl_2 \cdot 2NH_3$	18.6 ± 0.20	This work
235(337[a])	50	$MnCl_2 \cdot 6NH_3$	22.9 ± 0.32	This work
(278[a])		$MnCl_2 \cdot 2NH_3$	21.8 ± 0.25	This work
90(123[a])	30	$MnCl_2 \cdot 6NH_3$	11.5 ± 0.20	This work
(104[a])		$MnCl_2 \cdot 2NH_3$	10.8 ± 0.15	This work
120(188[a])	30	$MnCl_2 \cdot 6NH_3$	13.2 ± 0.21	This work
(147[a])		$MnCl_2 \cdot 2NH_3$	11.5 ± 0.15	This work
145(257[a])	30	$MnCl_2 \cdot 6NH_3$	14.1 ± 0.21	This work
(186[a])		$MnCl_2 \cdot 2NH_3$	12.7 ± 0.25	This work
165[a]	——	$MnCl_2 \cdot 6NH_3$	6.4	Mauran et al.[8]
285[a]	——	$MnCl_2 \cdot 6NH_3$	32.8	Mauran et al.[8]
350[a]	——	$MnCl_2 \cdot 6NH_3$	38.1	Mauran et al.[8]
150[a]	——	$MnCl_2 \cdot 2NH_3$	8.4	Mauran et al.[8]
235[a]	——	$MnCl_2 \cdot 2NH_3$	23.3	Mauran et al.[8]
320[a]	——	$MnCl_2 \cdot 2NH_3$	32.2	Mauran et al.[8]

[a]Densities were calculated with Eq. (18a) using the definition of Mauran et al.

Table 4 Effective thermal conductivities of graphite–$BaCl_2 \cdot 8NH_3$ complex[a]

ρ_b, kg/m^3	f_g, wt %	k_e, W/mK
100	50	16.9 ± 0.50
170	50	21.5 ± 0.25
215	50	23.3 ± 0.65
255	50	30.7 ± 0.35
75	30	9.63 ± 0.15
160	30	16.2 ± 0.55

[a]State of metallic salt $BaCl_2 \cdot 8NH_3$.

Table 4 shows the effective thermal conductivity of the graphite–$BaCl_2 \cdot 8NH_3$ complex from this work. The ammoniated state of $BaCl_2$ only exists as $BaCl_2 \cdot 8NH_3$. When f_g is 50%, thermal conductivity of the complex is in the range of 16.9–30.7 W/mK with bulk densities of 100–255 kg/m^3. When f_g is 30%, thermal conductivity is in the range of 9.6–16.2 W/mK with bulk densities of 75–160 kg/m^3. The overall behavior of the effective thermal conductivity is similar to the case of the graphite–$CaCl_2 \cdot nNH_3$ and $MnCl_2 \cdot nNH_3$ complexes. For all of the graphite–MS complexes investigated here, the effect of pressure of the ammonia gas on the effective thermal conductivity is negligible in comparison with other factors.

The preferred design for a reactor in a CHP frequently takes a cylindrical shape with the heat exchanger attached to the outer wall of the reactor as a form of a jacket. The heat transfer of the reactor can be characterized by thermal parameters.[6] The parameters that control the heat transfer in the reactor are the thermal resistance of the graphite–salt complex, the thermal resistance of the reactor wall, the thermal resistance between the wall and the complex, and the thermal resistance between heat transfer fluid and the wall. Overall heat transfer coefficient U_p can then be expressed as

$$(1/U_p) = (1/h_f) + (e_w/k_w) + (1/h_w) + (e_b/k_e) \qquad (19)$$

The value of h_f depends on many variables, such as fluid properties, system geometry, flow velocity, and so on. Generally, high h_f can be achieved with fluids, in particular, when evaporation or condensation is involved. For turbulent fluid flow of water, typical values are in the range of 2000–6000 W/m^2K (Ref. 6). If a gas is

used as the heat transfer fluid, the thermal resistance can be a critical factor. The thermal resistance of reactor wall (e_w/k_w), which is usually made of steel (~14 W/mK), can be neglected. Thus, the first and the second terms in Eq. (19) can be easily eliminated by an appropriate selection of the heat transfer fluid and the material of reactor. The value of h_w changes considerably with the degree of contact by initial filling of graphite–MS complex into the reactor and the extent of reaction. Therefore, the value of h_w can fluctuate over a wide range from 50 to 1000 W/m^{2}K (Refs. 6 and 8). In this work, the effective thermal conductivity of the graphite–MS complex is in the range of 10–49 W/mK, depending on the bulk density and the weight fraction of the graphite. For the reactor with a diameter of 20 cm, we can estimate the two thermal resistances, $1/h_w$ and e_b/k_{eff}. From simple calculations, the values of $1/h_w$ and e_b/k_{eff} are in the range of 2×10^{-2}–10^{-3} and 10^{-2}–2×10^{-3}, respectively. Thus, we know that the two thermal resistances affect the performance of the reactor to a same degree. The contact resistance between the complex and the wall can be reduced with a good contact. The thermal resistance of the graphite–MS complex decreases with a smaller diameter of the complex or with a higher thermal conductivity obtained by increasing the bulk density of the complex. However, the graphite–salt complex with high bulk density may suffer from the mass transfer problem that results from low gas permeability through the complex.[3] Optimum specifications for graphite–MS complexes, such as the bed thickness, the bulk density, the weight fraction of graphite, etc., should be determined by modeling the reactor that is coupled with chemical kinetics and heat and mass transfer. Such a work is ongoing in our laboratory.

Error Analysis

We consider the lateral heat loss by the external natural convection and by the radiation at the external surface of the specimen to validate the one-dimensional heat flow. The maximum heat loss by natural convection can be estimated by assuming the surface temperature of 332 K and the ambient temperature of 330 K. The dimension of the specimen is $5.5 \times 5.6 \times 10.0$ (mm^3). All properties such as β, k_f, ν, and Pr were evaluated at a mean film temperature of 331 K. Thus, the Rayleigh number is calculated as

$$Ra_L = Gr_L \cdot Pr = \frac{\beta \Delta T L^3}{\nu^3} Pr = \frac{(1/331)(2)(9.81)(10^{-2})^3(0.89)}{(17.9 \cdot 10^{-6})^3}$$

$$= 1.65 \cdot 10^2 \tag{20}$$

Because $Ra_L \ll 10^9$, the flow is laminar. From the definition by Churchill and Usagi (see Ref. 18), Prandtl number function ψ is evaluated as 0.383. Churchill and Usagi also correlated the average Nusselt number for the external natural flow on a vertical wall, and then the corresponding heat transfer coefficient was evaluated as

$$\bar{Nu}_L = 0.68 + 0.670 \cdot (Ra_L \cdot \psi)^{\frac{1}{4}} = 2.57 \tag{21a}$$

$$\bar{h}_L = (k/L)(\bar{Nu}_L) = 7.17\,\text{W/m}^2K \tag{21b}$$

Thus, the heat loss by natural convection is evaluated as

$$Q_{\text{conv}} = \bar{h}_L \cdot S \cdot (T_s - T_a) = 3.15 \times 10^{-3}\,\text{W} \tag{21c}$$

Because the specimen is completely enclosed by the ambient ammonia and the wall, the maximum radiative heat loss is evaluated as

$$Q_{\text{rad}} = \sigma \cdot S \cdot \left(T_s^4 - T_a^4\right) = 3.63 \times 10^{-3}\,\text{W} \tag{21d}$$

The heat liberation by the thermistor is evaluated using Eq. (11b) as 2.04×10^{-1} W. Therefore, heat loss by natural convection and radiation is at most 3.3% of the total heat liberation. However, actual heat loss is a much lower value because the temperature of the external surface during measurement is lower than 332 K, which is the temperature at the boundary between the thermistor and the specimen.

The error in the thermal conductivity resulting from current and voltage measurements is within 1.0%, which comes from the change of the heat flux by the variation of the thermistor's resistance, the intrinsic noise of the digital multimeter, the power supply, the resistance of the external circuit, etc. From the consideration of the total error analysis, the final precision of thermal conductivity measurements is estimated to be within 5.0%.

Conclusion

MS have been used as reactive materials for CHPs. Zeolite, active carbon, silica gel, etc., have been used as adsorbent materials for adsorption heat pumps (AHPs). These materials have a very low thermal conductivity of 0.1–0.5 W/mK, which made it impossible to transfer rapidly the thermal energy accompanied by the chemical reaction or adsorption to the heat transfer fluid. A number of methods have been considered to promote heat transfer in the reaction/adsorption bed. Accurate measurement of effective thermal conductivity has been essential to heat transfer analysis and to the dynamic simulation of reactor in CHPs.

Measurements of effective thermal conductivity were carried out in a specially designed apparatus that was built according to the transient one-dimensional heat flow method. The method developed in this work proved to be appropriate for measuring the effective thermal conductivity of reaction beds for CHPs. Moreover, we could also expect the measurement method to apply to other reaction beds for AHPs or metal hydride heat pump systems. The effective thermal conductivities of graphite–$CaCl_2$, $MnCl_2$, and $BaCl_2$ complexes were in the range of 10–49 W/mK depending on the bulk density, weight fraction of the graphite, and ammoniated state of the MS. Significant enhancement of heat transfer can be obtained using the graphite–MS complex, which results in a much shorter cycle time in the refrigeration and the heat pumping operations of CHPs. Thus, heat pump systems based on these materials are expected to provide an alternative to compression machines that use environmentally unfavorable CFCs and HCFCs as working fluids.

Acknowledgments

The authors are pleased to acknowledge the financial assistance of the Korea Science and Engineering Foundation (Project 95-0502-04-01-3) and the Pohang Iron and Steel Company, Ltd. (Project 1-UD-97012-01).

References

[1] Spinner, B., "Ammonia-Based Thermochemical Transformers," *Heat Recovery Systems and CHP*, Vol. 13, No. 4, 1993, pp. 301–307.

[2] Mazet, N., and Amouroux, M., "Analysis of Heat Transfer in a Non-isothermal Solid-Gas Reacting Medium," *Chemical Engineering Community*, Vol. 99, No. 1, 1991, pp. 175–200.

[3] Lu, H.-B., Mazet, N., and Spinner, B., "Modelling of Gas-Solid Reaction-Coupling of Heat and Mass Transfer with Chemical Reaction," *Chemical Engineering Science*, Vol. 51, No. 15, 1996, pp. 3829–3845.

[4] Stitou, D., and Crozat, G., "Dimensioning Nomograms for the Design of Fixed-Bed Solid-Gas Thermochemical Reactors with Various Geometrical Configurations," *Chemical Engineering and Processing*, Vol. 36, No. 1, 1997, pp. 45–58.

[5] Goetz, V., Elie, F., and Spinner, B., "The Structure and Performance of Single Effect Solid-Gas Chemical Heat Pumps," *Heat Recovery Systems and CHP*, Vol. 13, No.1, 1993, pp. 79–96.

[6] Groll, M., "Reaction Beds for Dry Sorption Machine," *Heat Recovery Systems and CHP*, Vol. 13, No. 4, 1993, pp. 341–346.

[7] Han, J. H., Cho, K. W., Lee, K.-H., and Kim, H., "Porous Graphite Matrix for Chemical Heat Pumps," *CARBON*, Vol. 36, No. 12, 1998, pp. 1801–1810.

[8] Mauran, S., Prades, P., and L'Haridon, F., "Heat and Mass Transfer in Consolidated Reacting Beds for Thermochemical Systems," *Heat Recovery Systems and CHP*, Vol. 13, No. 4, 1993, pp. 315–319.

[9] Goetz, V., and Marty, A., "A Model for Reversible Solid-Gas Reactions Submitted to Temperature and Pressure Constraints," *Chemical Engineering Science*, Vol. 47, No. 17, 1992, pp. 4445–4454.

[10] Han, J. H., Cho, K. W., Lee, K.-H., and Kim, H., "Transient One-Dimensional Heat Flow Technique Applied to Porous Reactive Medium," *Review of Scientific Instrument*, Vol. 69, No. 8, 1998, pp. 3079–3080.

[11] Carslaw, H. S., and Jaeger, J. C., *Conduction of Heat in Solids*, Oxford Univ. Press, Oxford, 1959, p. 112.

[12]Wentworth, W. E., Johnston, D. W., and Raldow, W. M., "Chemical Heat Pumps Using a Dispersion of a Metal Salt Ammoniate in an Inert Solvent," *Solar Energy*, Vol. 26, No. 2, 1981, pp. 141–146.

[13]Furrer, M., "Thermoanalytische Untersuchung Ausgewaehlter Komplexe Von Anorganischen Chloriden Mit Ammoniak und Ammoniak-Derivaten," Eidg. Inst. für Reaktorforschung, Bericht Nr. 392, Würenlingen-Schweiz, April 1980.

[14]Hosatte, S., and Rheault, F., "Kinetics and Modelling of $CaCl_2$-NH_3 Reactions," *Proceeding of the Symposium of Solid Sorption Refrigeration*, Vol. 1, LIMSI, Paris, 1992, pp. 245–252.

[15]Marty, A., "Etude par Microcalorimeterie de la Reactivite de Deux Ammoniacates de Chlorure de Manganese," *Journal of Thermal Analysis*, Vol. 37, No. 3, 1991, pp. 479–498.

[16]Lepinasse, E., and Spinner, B., "Cold Production Through Coupling of Solid-Gas Reactors," *International Journal of Refrigeration*, Vol. 17, No. 5, 1994, pp. 309–322.

[17]Valkov, V., "Measurement of Technique for Determination of Thermochemical Properties of Thermochemical Storage Materials," *Experimental Heat Transfer, Fluid Mechanics and Thermodynamics*, Vol. 12, No. 6, 1993, pp. 529–536.

[18]Mills, A. F., "Heat Transfer," *Convection Fundamentals and Correlations*, 1st ed., Irwin, Boston, 1992, pp. 293–294.